RESEARCH ARTICLE | AUGUST 26 2024

Temperature-dependent dielectric behavior of $A_6B_2O_{17}$ (A = Zr, Hf; B = Nb, Ta) phases \bigcirc

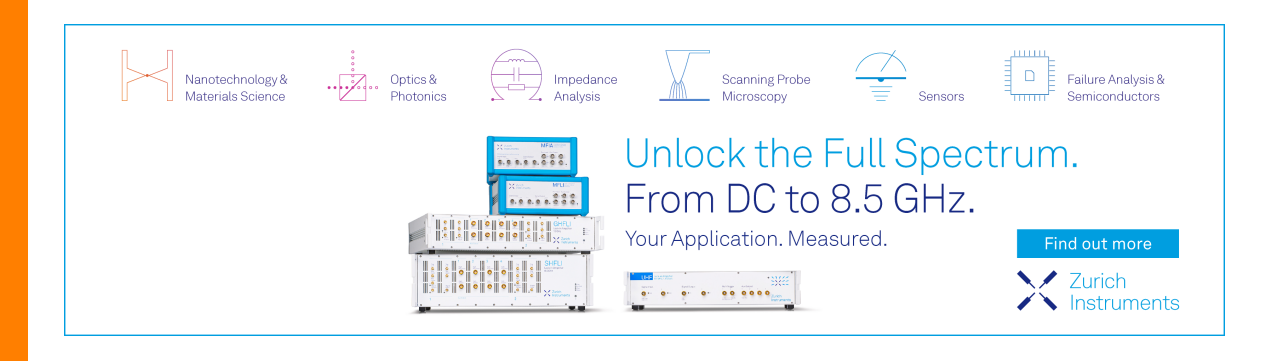
R. Jackson Spurling **▼** ⑩ ; Michael T. Marakovits ⑪ ; Arafat Hossain ⑫ ; Saeed S. I. Almishal ⑫ ; Steven E. Perini ⑩ ; Michael T. Lanagan ⑫ ; Jon-Paul Maria



Appl. Phys. Lett. 125, 092901 (2024) https://doi.org/10.1063/5.0219964









Cite as: Appl. Phys. Lett. **125**, 092901 (2024); doi: 10.1063/5.0219964 Submitted: 21 May 2024 · Accepted: 9 July 2024 · Published Online: 26 August 2024











AFFILIATIONS

- Department of Materials Science and Engineering, Pennsylvania State University, 215 Steidle Building, 1 Pollock Road, Steidle Building, University Park, Pennsylvania 16802, USA
- ²Department of Engineering Science and Mechanics, Pennsylvania State University, N-329 Millenium Science Complex, University Park, Pennsylvania 16802, USA
- ³Department of Electrical Engineering, Pennsylvania State University, N-329 Millenium Science Complex, University Park, Pennsylvania 16802, USA
- ⁴Materials Research Institute, Pennsylvania State University, N-260 Millenium Science Complex, University Park, Pennsylvania 16802, USA
- ⁵Department of Materials Science and Engineering, Pennsylvania State University, 407 Steidle Building, 1 Pollock Road, Steidle Building, University Park, Pennsylvania 16802, USA

ABSTRACT

We report on temperature-dependent dielectric behavior of disordered ternary $A_6B_2O_{17}$ (A = Zr, Hf; B = Nb, Ta)-form oxides in the GHz frequency range. The microwave dielectric properties including relative permittivity, dielectric loss, and temperature-dependent relative permittivity were characterized using cylindrical dielectric resonators using a resonant post measurement technique. Dielectric measurements through the resonant post method approach generally agree with dielectric measurements of $A_6B_2O_{17}$ bulk ceramics measured through standard resonant post techniques. Coefficients describing the temperature-dependent relative permittivity for ternary $A_6B_2O_{17}$ phases are strongly positive, suggesting contributions to polarizability arising from long-range mechanisms potentially associated with structural disorder. These observations support the working hypothesis that material functionality can be engineered by the chemical diversity and structural disorder possible in high configurational entropy $A_6B_2O_{17}$ phases.

Published under an exclusive license by AIP Publishing. https://doi.org/10.1063/5.0219964

The $A_6B_2O_{17}$ (A=Zr, Hf; B=Nb, Ta) phases have captured the ceramics community's interest due to their complex structure, which tolerates substantial atomic disorder and chemical diversity (Fig. 1).^{1–4} Foundational reports^{2–4} demonstrate the entropic contribution to structural stability and pave the way for property studies. While substantial attention is fixed on $A_6B_2O_{17}$ high-temperature thermal and chemical transport and mechanical properties, ^{5–8} recent reports high-light opportunities for these phases as electronic materials. Microwave frequency dielectric properties suggest promise for electroceramic applications, but characterization has hitherto been limited to room-temperature performance.

As discussed by Harrop, ¹² materials tend to exhibit temperaturedependent relative permittivity behavior underpinned by fundamental differences in structure and bonding. Therefore, relative permittivity temperature coefficient measurements form a phenomenological basis for classifying materials. Comparisons between materials with dissimilar dielectric behavior will highlight any unique property effects derived from chemistry and structure. The recent focus on entropic contributions to material structure and performance gives heightened importance to fundamental property studies for disordered systems. $^{\bar{1}3-15}$ Characterizing the temperature-dependence of relative permittivity in $A_6B_2O_{17}$ represents an important opportunity for entropy-assisted electroceramics engineering. We report on temperature-dependent bulk dielectric properties of ternary $A_6B_2O_{17}$ phases and contextualize their performance relative to similar crystalline ionic inorganics; we discuss connections between structural disorder and dielectric properties.

Bulk ceramics are synthesized via solid-state reactive sintering as described in the literature.⁴ Stoichiometric amounts of as-received

a) Author to whom correspondence should be addressed: rjs7012@psu.edu

oxide powders (ZrO₂, TOSOH, 99.87%; Nb₂O₅, Sigma Aldrich, 99.99%; HfO₂, Sigma Aldrich, 98%; Ta₂O₅, Sigma Aldrich, 99.5%) are ball milled in methanol (Fisher Scientific, Grade: Certified ACS Reagent) using yttrium-stabilized zirconia media for 30 h, followed by air drying at $100\,^{\circ}$ C to drive off methanol for at least 2 h.

Powders are compacted via uniaxial pressing at \sim 172 MPa (\sim 25 000 psi) in a 0.5 in. diameter steel die to form \sim 2 g green bodies and are subsequently sintered in air at 1500 °C for 12 h. Reacted pellets are examined with x-ray diffraction (Panalytical Empyrean, Bragg-Brentano optic, θ –2 θ geometry, Cu k α source λ =1.54 Å) to confirm $A_6B_2O_{17}$ phase formation. Approximate density measurements are made using calipers to confirm small volume fraction porosity for reliable dielectric measurements.

Separately, reference samples of TiO_2 and $CaTiO_3$ (for which dielectric properties have previously been well-characterized) are synthesized; these serve as comparison metrics for the $A_6B_2O_{17}$ phases. As-received powders (Alfa Aesar) for each reference sample are compacted under \sim 62 MPa (\sim 9000 psi) pressure to form \sim 0.5-in. diameter green bodies. These are subsequently sintered at 1600 °C for 24 h.

Relative permittivity and dielectric loss were characterized for a ceramic, cylindrical resonator using the TE_{011} mode, whereas the

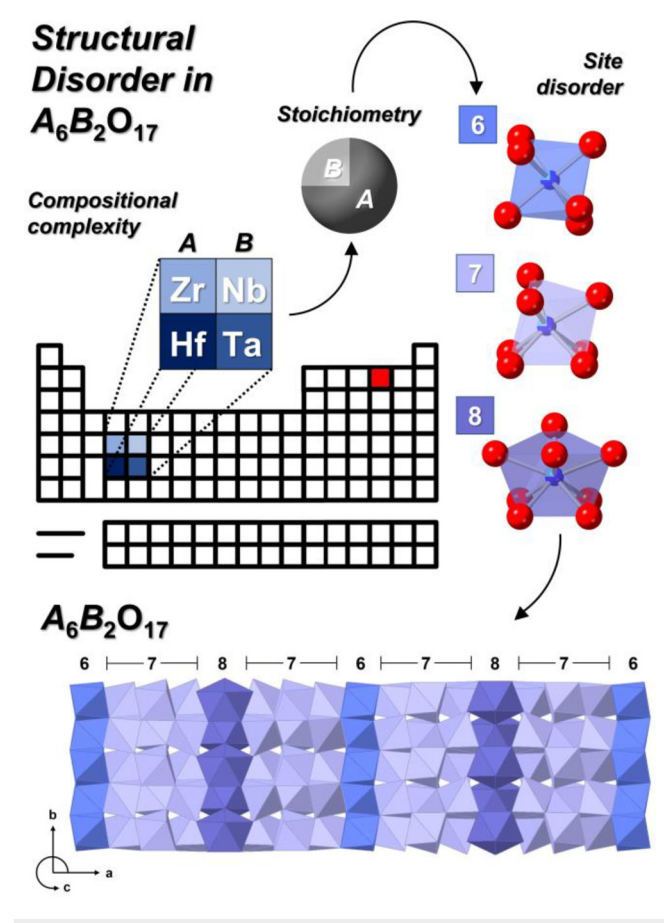


FIG. 1. $A_6B_2O_{17}$ model highlighting structural disorder (CrystalMaker® model adapted from Spurling, 11 structure solution by Galy and Roth 1 and McCormack and Kriven 2).

temperature-dependent relative permittivity coefficient was determined from a resonant post inside a cavity using the similar $TE_{01\delta}$ mode. For the temperature-dependent measurements, samples are individually placed on a Styrofoam substrate inside a silver-painted fused silica cylindrical cavity to prevent thermal expansion. A metallic plate screwed into the sample cavity provides boundary conditions for measuring the $TE_{01\delta}$ mode. The sample cavity is connected via coaxial cables to a vector network analyzer, which records sample resonant peaks at the $TE_{01\delta}$ mode from which relative permittivity is calculated (see the supplementary material). The sample cavity sits on a hot plate, which is adjusted for elevated temperature measurements at 50, 75, and 100 °C. An additional (empty) sample cavity is situated on the hot plate adjacent to the active sample cavity; this empty cavity is connected to an isolated thermocouple, which provides accurate temperature monitoring. This setup is diagramed in the supplementary material.

X-ray diffraction results (Fig. 2) confirm near-complete reactions in $A_6B_2O_{17}$ ternary ceramics under the given thermal budget, similar to other literature reports. More refractory systems (i.e., $Hf_6Ta_2O_{17}$ and $Hf_6Nb_2O_{17}$) possess larger residual precursor phase fractions as indicated by the secondary diffraction peaks. Logarithmic XRD plotting amplifies low-intensity residual precursor peaks. Prior literature reports diminishing returns for $A_6B_2O_{17}$ yield above a \sim 96 wt. % threshold from solid-state powder reactions at high synthesis temperatures (e.g., \geq 1200 °C). Achieving higher yields may require long hold times at elevated temperatures or successive milling and resintering. Nonetheless, ceramics are sufficiently well-reacted for accurate $A_6B_2O_{17}$ property characterization.

With the exception of $Hf_6Ta_2O_{17}$, sintered pellets are dense (>95% $\rho_{Theoretical}$) with minimal anticipated contributions from porosity to measured relative permittivity for the $Zr_6Nb_2O_{17}$, $Zr_6Ta_2O_{17}$, and $Hf_6Nb_2O_{17}$ permutations; $Hf_6Ta_2O_{17}$ is difficult to densify under these sintering conditions, though other reports observe densification at higher temperatures. Scanning electron microscopy (supplementary material) highlights densified microstructures in polished sintered

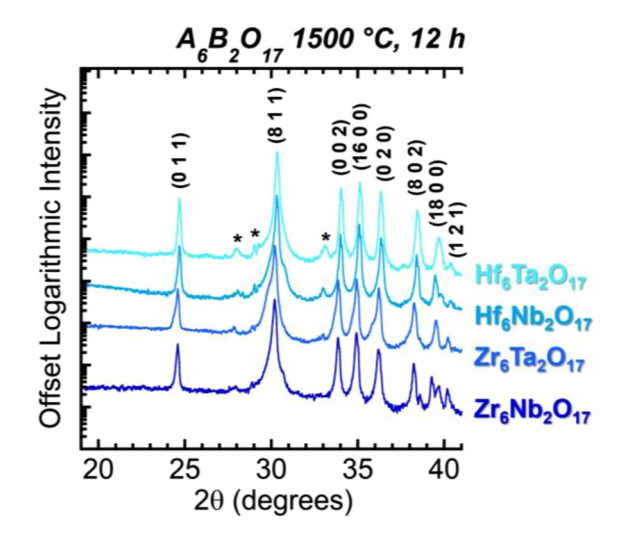


FIG. 2. XRD scans indicate high-temperature $A_6B_2O_{17}$ phase stabilization for each ternary composition. Residual precursor peaks labeled (*).

ceramics with relatively small, isolated internal porosity in $\rm Zr_6Nb_2O_{17}$, $\rm Zr_6Ta_2O_{17}$, and $\rm Hf_6Nb_2O_{17}$; $\rm Hf_6Ta_2O_{17}$ is under-dense and has a much larger evident volumetric fraction of porosity. Companion energy dispersive spectroscopy confirms compositional homogeneity and approximate stoichiometry for sintered ternary $A_6B_2O_{17}$ ceramics (supplementary material). This suggests that any secondary diffraction peaks as observed by XRD are associated with small, dispersed fractions of unreacted precursor phase from the as-received powders; this is consistent with other literature reports for high-temperature solid-state $A_6B_2O_{17}$ reactive sintering. $^{4.7,10,16}$

Based on this structural data, we conclude that the $\rm Zr_6Nb_2O_{17}$, $\rm Zr_6Ta_2O_{17}$, and $\rm Hf_6Nb_2O_{17}$ ceramics are sufficiently reacted and densified for reliable dielectric property measurements. $\rm Hf_6Ta_2O_{17}$ is also well-reacted but possesses a much lower relative density and higher internal porosity. We still report dielectric data for $\rm Hf_6Ta_2O_{17}$ and observe a similar temperature-dependent dielectric phenomenological behavior as the companion ternary phases; however, due to this larger porosity, we note a much lower magnitude for the measured relative permittivity.

Figure 3 shows relative permittivity measurements and resonant frequencies as a function of temperature for each ternary $A_6B_2O_{17}$ permutation measured in the GHz frequency range. Measurements in this frequency regime will include polarization from ionic and electronic mechanisms and exclude any interfacial or orientational effects. Overall, relative permittivity values are similar to measurements for ${\rm Zr_6Nb_2O_{17}}$ and ${\rm Zr_6Ta_2O_{17}}$ using a standard Hakki-Coleman approach. 10,17 Measured relative permittivities are strongly linear with temperature across the tested range. Based on prior classifications by Harrop 12 and $A_6B_2O_{17}$ room-temperature dielectric measurements, 10 we anticipate a large negative temperature-dependent relative permittivity coefficient (${\rm TC}\varepsilon_{\rm r}\approx -500$) typical for an ionic paraelectric.

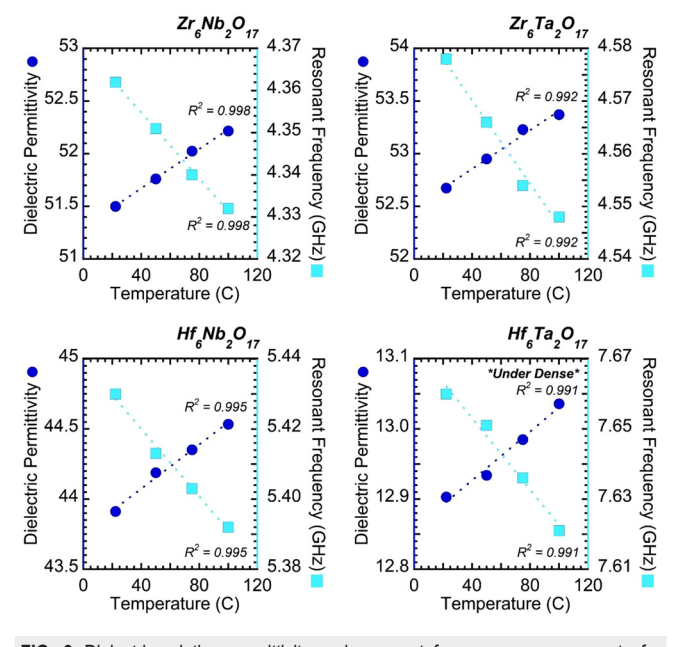


FIG. 3. Dielectric relative permittivity and resonant frequency measurements for $A_6B_2O_{17}$ samples as a function of temperature.

Surprisingly, we observe a strongly positive temperature coefficient $(TC\varepsilon_r)$ for each ternary $A_6B_2O_{17}$ permutation (Table I).

To contextualize and validate these results, we measured temperature coefficients for similar known oxides including TiO2 and CaTiO₃. We select these materials as comparison metrics because they are high ε_r dielectrics with similar ionic bonding character to $A_6B_2O_{17}$ (see the supplementary material). As ionic paraelectrics, they should have large negative temperature coefficients, similar to (albeit larger than) expected values for the A₆B₂O₁₇ phases. Additionally, measurements for ordered structures like TiO2 and CaTiO3 will highlight dielectric anomalies associated with a disordered structure as in A₆B₂O₁₇. TiO₂ and CaTiO₃ measurements (Table I) are consistent with literature reports 12,18,19 for each oxide and fall within expected ranges for paraelectrics based on Harrop's classifications. While TiO₂ and CaTiO₃ possess large relative permittivities and similar ionic bonding character to $A_6B_2O_{17}$ (see the supplementary material), both exhibit large negative temperature coefficients typical for ionic paraelectrics; these data contrast with $A_6B_2O_{17}$ results.

Both Harrop's report ¹² and Bosman and Havinga's study on cubic ionic compounds ²⁰ show that most conventional solid-state high ε_r materials should exhibit a negative temperature-dependent relative permittivity coefficient (Fig. 4). The large positive temperature coefficients exhibited by $A_6B_2O_{17}$ phases are, therefore, uncharacteristic of high ε_r ionic inorganics. This dissimilarity is underscored by contrasting results for $A_6B_2O_{17}$ and both TiO₂ and CaTiO₃. The unique $A_6B_2O_{17}$ response must arise from an intrinsic polarization mechanism associated with the chemistry and structure, which remains active in the high frequency (GHz) regime. Isolating the precise mechanism driving this behavior in $A_6B_2O_{17}$ is challenging, not least because it likely derives from structural factors which are not relevant in materials examined in some prior reports. ^{12,20} However, comparisons between ordered and disordered structures give us a basis for assessing unique property behaviors in $A_6B_2O_{17}$.

Positive relative permittivity temperature coefficients have been documented in other systems, including bismuth-based pyrochlore-derivative niobates and tantalates, $^{21-24}$ alkaline-earth and rare-earth zirconates, $^{25-27}$ and disordered glasses. 12 Unique local crystal structure contributes to positive temperature-dependent relative permittivity coefficients in these materials; in orthohombic (perovskite-derivative) CaZrO₃ and SrZrO₃, for example, tilting by ZrO₆ octahedra at elevated temperatures has been suggested to drive additional polarization, resulting in a positive TCs_r. 26,27 Cockbain and Harrop note that structural disorder is associated with wide distributions in relaxation times

TABLE I. Dielectric relative permittivity and temperature coefficient measurements for each A₆B₂O₁₇ permutation as well as crystalline inorganic reference samples.

Material	Slope of ε_r vs T (1/°C)	Avg. Meas. $\varepsilon_{ m r}$	$TC\varepsilon_{r}$ (ppm/°C)
$Zr_6Nb_2O_{17}$	0.0093	52	179
$Zr_6Ta_2O_{17}$	0.0092	53	173
$Hf_6Nb_2O_{17}$	0.0079	44	179
$Hf_6Ta_2O_{17}$	0.0017	13	131
TiO ₂ (rutile) CaTiO ₃ (perovskite)	-0.0653 -0.1743	83 121	-787 -1446

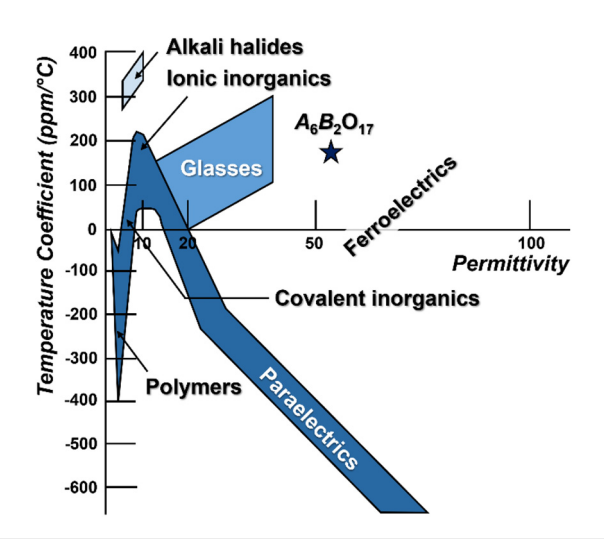


FIG. 4. Reproduction of the temperature coefficient plot by Harrop ¹² with permission from Springer Nature with $A_6B_2O_{17}$ superimposed. $A_6B_2O_{17}$ phases exhibit temperature-dependent dielectric behavior, which is atypical of ionic inorganics in this regime.

resulting in unique macroscopic temperature-dependent dielectric responses. 28 We propose that the disorder and unique local coordinations in the $A_6B_2O_{17}$ structure could contribute to long-range polarization mechanisms, which change the temperature-dependent dielectric response.

The temperature-dependent derivative of the Clausius–Mossotti Equation provides a mathematical basis for identifying structure-derived contributions to $TC\varepsilon_r$. The Clausius–Mossotti Equation defines the relation between relative permittivity (ε) and the total polarizability of constituent ionic species (α) in a defined volume (V),

$$\frac{\varepsilon - 1}{\varepsilon + 2} = \frac{\alpha}{3V\varepsilon_0}. (1)$$

An initial treatment by Havinga²⁹ identified the following temperature-dependent Clausius–Mossotti Equation derivative at constant pressure:

$$\frac{1}{\varepsilon} \left(\frac{\partial \varepsilon}{\partial T} \right)_{p} = \frac{(\varepsilon - 1)(\varepsilon + 2)}{\varepsilon} \left[\left[-\frac{1}{3V} \left(\frac{\partial V}{\partial T} \right)_{p} \right] + \left[\frac{1}{3\alpha} \left(\frac{\partial \alpha}{\partial V} \right)_{T} \left(\frac{\partial V}{\partial T} \right)_{p} \right] + \left[\frac{1}{3\alpha} \left(\frac{\partial \alpha}{\partial T} \right)_{V} \right] \right] \\
= \frac{(\varepsilon - 1)(\varepsilon + 2)}{\varepsilon} (A + B + C). \tag{2}$$

Equation (2) highlights three factors impacting the temperature-dependent dielectric constant: (*A*) the decrease in polarizable particles per unit volume as a result of thermal expansion, (*B*) the increase in particle polarizability for a fixed number of particles contained in an increasing volume with increasing temperature, and (*C*) the temperature-dependence of polarizability at fixed volume.

While this treatment is sufficient for ordered isotropic cubic materials (such as the alkali halide salts examined by Havinga²⁹ and Bosman and Havinga²⁰), Cockbain and Harrop²⁸ note the limitations

inherent in applying this approach to disordered materials. They propose an additional term (*D*) encompassing polarization contributions from disorder and defect-related mechanisms,

$$\frac{1}{\varepsilon} \left(\frac{\partial \varepsilon}{\partial T} \right)_p = D = K \tan \delta \approx 0.05 \tan \delta. \tag{3}$$

The K parameter (which encompasses relaxation times for a given defect or disorder feature) has slightly different forms in initial derivations by Gevers³⁰ and Hersping;³¹ however, in both cases, $K\approx 0.05\,^{\circ}\mathrm{C}^{-1}$. Cockbain and Harrop²⁸ present an additional fifth "E" term comprising relaxation times of certain dipoles, which impacts the relative permittivity behavior with temperature; however, they note that this has limited applicability across most systems and so, given our current focus on the disorder D term, we refer the reader to the literature for additional detailed discussions. Equation (3) demonstrates that contributions to dielectric loss arising from disordered states will impact the magnitude of the temperature-dependent relative permittivity coefficient.

Noticeably, this D term neither appears in derivations for nor is needed in the explanation of temperature-dependent relative permittivity coefficients for simple ordered materials, such as the alkali halides. However, for disordered systems, including $A_6B_2O_{17}$, this D term becomes significant. Mechanistically, the disordered structure can produce localized dipole states, which supply an additional polarization mechanism not present in ordered materials. The effect of these dipole states on the overall temperature-dependent relative permittivity behavior can be easily observed in the high frequency (GHz) range, since active dielectric polarizability contributions are limited to ionic and electronic phenomena. The loss tangent values for $A_6B_2O_{17}$ and CaTiO₃ and TiO₂ reference samples are presented for each temperature in Table II. We note that the loss values for each ternary $A_6B_2O_{17}$ permutation are an order of magnitude higher than both the CaTiO₃ and TiO2 reference samples; moreover, the D term magnitude obtained for $A_6B_2O_{17}$ (assuming $\tan\delta \approx 0.002$) is 100 ppm/°C, which is the same order of magnitude as the TC ε_r for each $A_6B_2O_{17}$ permutation. Therefore, the D term magnitude is large for $A_6B_2O_{17}$ (compared to relatively small values for ordered CaTiO₃ and TiO₂) and could be sufficient to drive $TC\epsilon_{\rm r}$ positive. Overall, this behavior is consistent with expectations assuming activity from disorder-based polarization mechanisms represented in Eq. (3). These results highlight key connections between the unique structure and material properties of disordered $A_6B_2O_{17}$ phases.

Our results, coupled with the experimental observations for chemical relatives and the mathematical theory support, suggest strong connections between structure (manifesting both as sublattice disorder and unique local coordination environments) and electronic properties in $A_6B_2O_{17}$ phases. However, because this structure combines unique coordination environments with substantial cation sublattice disorder, there are likely complex, multi-faceted contributions to the structure–property relationships studied here. Therefore, further studies are merited focusing on local structure in the $A_6B_2O_{17}$ phases.

As noted by Harrop, 12 materials that exhibit anomalous temperature-dependent relative permittivity often display other unique, frequently nonlinear, electronic properties. Additionally, any disorder and structure contributions to the $A_6B_2O_{17}$ temperature-dependent permittivity behavior may be realized in other high-entropy or disordered oxides, making this a potential area for further study.

TABLE II. Loss tangent measurements for each A₆B₂O₁₇ permutation and reference samples.

Material	RT tan δ	50 °C tan δ	75 °C tan δ	100 °C tan δ	Avg. $\tan \delta$
$Zr_6Nb_2O_{17}$	0.002 16	0.002 11	0.002 12	0.002 11	0.002 13
$Zr_6Ta_2O_{17}$	0.002 33	0.002 33	0.002 26	0.002 25	0.002 29
$Hf_6Nb_2O_{17}$	0.00172	0.00174	0.00175	0.00175	0.00174
$Hf_6Ta_2O_{17}$	0.002 53	0.002 19	0.001 92	0.001 80	0.002 11
TiO ₂ (rutile)	0.000 80	0.00078	0.000 82	0.000 86	0.00081
CaTiO ₃ (perovskite)	0.000 59	0.000 63	0.000 69	0.00073	0.00066

Further research can identify specific mechanisms associated with the structural disorder, which produce this unique contribution to temperature-dependent permittivity behavior. However, regardless of the exact mechanism at play, these results demonstrate that the unique characteristics of $A_6B_2O_{17}$ phases are not relegated simply to structure. This opens the door to electronic property exploration in $A_6B_2O_{17}$ phases and other oxides with a focus on disorder-assisted materials design for emerging functional electroceramics.

We report a strong positive temperature dependence of dielectric permittivity in $A_6B_2O_{17}$ (A=Zr, Hf; B=Nb, Ta) disordered oxides. This anomalous behavior contrasts with similar ionic inorganics such as TiO₂ and CaTiO₃, which adopt strongly negative temperature coefficients. This suggests long-range mechanistic contributions to polarizability likely associated with the $A_6B_2O_{17}$ disordered structure and unique local environments. $A_6B_2O_{17}$ shows increasing promise for electroceramic material applications and merit continued investigation.

See the supplementary material for further discussions/diagram of the experimental setup for bulk temperature-dependent permittivity measurements; scanning electron microscopy and energy dispersive spectroscopy microstructure and chemical analysis for the sintered bulk ceramics; and basic ionic bond calculations.

This material is based upon work supported by the National Science Foundation, as part of the Center for Dielectrics and Piezoelectrics under Grant Nos. IIP-1841453 and IIP1841466. The authors also gratefully acknowledge support from NSF MRSEC DMR-2011839. R.J.S. was supported by the National Science Foundation Graduate Research Fellowship Program under Grant No. DGE1255832. Any opinions, findings, and conclusions or recommendations expressed in this material are those of the authors and do not necessarily reflect the views of the National Science Foundation. The authors appreciate assistance from Erik Furton (Penn State) with ceramic polishing.

AUTHOR DECLARATIONS Conflict of Interest

The authors have no conflicts to disclose.

Author Contributions

R. Jackson Spurling: Conceptualization (equal); Data curation (equal); Formal analysis (equal); Investigation (equal); Methodology (equal);

Writing - original draft (equal); Writing - review & editing (equal). Michael T. Marakovits: Data curation (equal); Formal analysis (equal); Investigation (equal); Methodology (equal); Validation (equal); Writing - review & editing (equal). Arafat Hossain: Data curation (equal); Formal analysis (equal); Methodology (equal); Validation (equal); Writing - review & editing (equal). Saeed S. I. Almishal: Conceptualization (supporting); Formal analysis (supporting); Writing - review & editing (equal). Steven Perini: Formal analysis (supporting); Methodology (supporting); Writing - review & editing (supporting). Michael T. Lanagan: Conceptualization (equal); Formal analysis (equal); Investigation (equal); Methodology (equal); Project administration (equal); Supervision (equal); Validation (equal); Writing review & editing (equal). Jon-Paul Maria: Conceptualization (equal); Formal analysis (equal); Funding acquisition (equal); Investigation (equal); Methodology (equal); Project administration (equal); Supervision (equal); Writing – review & editing (equal).

DATA AVAILABILITY

The data that support the findings of this study are available within the article and its supplementary material.

REFERENCES

- ¹J. Galy and R. S. Roth, "The crystal structure of Nb₂Zr₆O₁₇," J. Solid State Chem. 7, 277 (1973).
- ²S. J. McCormack and W. M. Kriven, "Crystal structure solution for the $A_6B_2O_{17}$ (A = Zr, Hf; B = Nb, Ta) superstructure," Acta Crystallogr. 75, 227 (2019).
- ³A. A. Voskanyan, K. Lilova, S. J. McCormack, W. M. Kriven, and A. Navrotsky, "A new class of entropy stabilized oxides: Commensurately modulated $A_6B_2O_{17}$ (A = Zr, Hf; B = Nb, Ta) structures," Scr. Mater. **204**, 114139 (2021).
- ⁴R. J. Spurling, C. Skidmore, N. S. McIlwaine, and J.-P. Maria, "Phase equilibria and metastability in the high-entropy $A_6B_2O_{17}$ oxide family with A = Zr, Hf and B = Nb, Ta," J. Mater. Sci. **58**, 6164–6173 (2023).
- ⁵Z. Y. Tan, Z. H. Yang, W. Zhu, L. Yang, Y. C. Zhou, and X. P. Hu, "Mechanical properties and calcium-magnesium-alumino-silicate (CMAS) corrosion behavior of a promising Hf₆Ta₂O₁₇ ceramic for thermal barrier coatings," Ceram. Int. 46, 25242 (2020).
- ⁶H. Li, Y. Yu, B. Fang, P. Xiao, W. Li, and S. Wang, "Calcium-magnesium-alumina-silicate (CMAS) corrosion behavior of A₆B₂O₁₇ (A=Zr, Hf; B=Nb, Ta) as potential candidate for thermal barrier coating (TBC)," Corros. Sci. 204, 110395 (2022).
- $^7\mathrm{Q}.$ Yang, H. Charalambous, E. M. Sobalvarro, J. Rivera, P. W. F. Evans, J. T. Cahill, W. L. Du Frane, and J. D. Kuntz, "Synthesis, sintering, and grain growth kinetics of $\mathrm{Hf_6Ta_2O_{17}}$," J. Eur. Ceram. Soc. $43,\,4541$ (2023).
- 8 J. Y. Wu, X. P. Hu, S. Liu, Q. Liu, J. W. Guo, S. Wang, S. Han, and W. Zhu, "High-temperature mechanical properties and fracture mechanism of $A_6B_2O_{17}$

- (A= Hf, Zr; B= Ta, Nb) high-entropy ceramics," J. Eur. Ceram. Soc. 44, 3652 (2024).
- ⁹T. Miruszewski, A. Mielewczyk-Gryń, D. Jaworski, W. F. Rosenberg, S. J. McCormack, and M. Gazda, "Charge transport in the $A_6B_2O_{17}$ (A=Zr, Hf; B=Nb, Ta) superstructure series," J. Electrochem. Soc. 171, 034503 (2024).
- 10 R. J. Spurling, S. S. I. Almishal, J. Casamento, J. Hayden, R. Spangler, M. Marakovits, A. Hossain, M. Lanagan, and J. Maria, "Dielectric properties of disordered $A_6B_2O_{17}\ (A=Zr;\ B=Nb,\ Ta)\ phases,"$ J. Am. Ceram. Soc. (published online 2024).
- ¹¹R. J. Spurling, "Entropy-inspired materials design for next-generation electroceramics," Am. Ceram. Soc. Bull. **103**, 40 (2024).
- ¹²P. J. Harrop, "Temperature coefficients of capacitance of solids," J. Mater. Sci. 4, 370 (1969)
- ¹³A. Sarkar, B. Breitung, and H. Hahn, "High entropy oxides: The role of entropy, enthalpy and synergy," Scr. Mater. 187, 43 (2020).
- ¹⁴G. N. Kotsonis, S. S. I. Almishal, F. M. dos Santos Vieira, V. H. Crespi, I. Dabo, C. M. Rost, and J.-P. Maria, "High-entropy oxides: Harnessing crystalline disorder for emergent functionality," J. Am. Ceram. Soc. 106, 5587 (2023).
- ¹⁵R. J. Spurling, E. A. Lass, X. Wang, and K. Page, "Entropy-driven phase transitions in complex ceramic oxides," Phys. Rev. Mater. 6, 090301 (2022).
- ¹⁶H. Charalambous, M. H. Jancich, P. W. F. Evans, J. Rivera, J. T. Cahill, W. L. Du Frane, J. D. Kuntz, and B. Yang, "Processing and characterization of the homologous Zr_xTa₂O_{2x+5} series," Ceram. Int. 50, 15848 (2024).
- 17B. W. Hakki and P. D. Coleman, "A dielectric resonator method of measuring inductive capacities in the millimeter range," IEEE Trans. Microwave Theory Tech. 8, 402 (1960).
- ¹⁸W. Luo, J. Guo, C. Randall, and M. Lanagan, "Effect of porosity and microstructure on the microwave dielectric properties of rutile," Mater. Lett. 200, 101 (2017).
- ¹⁹K. Haines, T. Neuberger, M. Lanagan, E. Semouchkina, and A. G. Webb, "High Q calcium titanate cylindrical dielectric resonators for magnetic resonance microimaging," J. Magn. Reson. 200, 349 (2009).

- ²⁰A. J. Bosman and E. E. Havinga, "Temperature dependence of dielectric constants of cubic ionic compounds," Phys. Rev. 129, 1593 (1963).
- ²¹D. Liu, Y. Liu, S. Huang, and X. Yao, "Phase structure and dielectric properties of Bi₂O₃-ZnO-Nb₂O₅-based dielectric ceramics," J. Am. Ceram. Soc. 76, 2129 (1993).
- 22X. Wang, H. Wang, and X. Yao, "Structures, phase transformations, and dielectric properties of pyrochlores containing bismuth," J. Am. Ceram. Soc. 80, 2745 (1997).
- 23S. Kamba, V. Porokhonskyy, A. Pashkin, V. Bovtun, J. Petzelt, J. C. Nino, S. Trolier-McKinstry, M. T. Lanagan, and C. A. Randall, "Anomalous broad dielectric relaxation in Bi_{1.5}Zn_{1.0}Nb_{1.5}O₇ pyrochlore," Phys. Rev. B 66, 054106 (2002).
- ²⁴H. Youn, T. Sogabe, C. A. Randall, T. R. Shrout, and M. T. Lanagan, "Phase relations and dielectric properties in the Bi₂O₃–ZnO–Ta₂O₅ system," J. Am. Ceram. Soc. 84, 2557 (2001).
- ²⁵H. Stetson and B. Schwartz, "Dielectric properties of zirconates," J. Am. Ceram. Soc. 44, 420 (1961).
- 26R. C. Kell, A. C. Greenham, and G. C. E. Olds, "High-permittivity temperature-stable ceramic dielectrics with low microwave loss," J. Am. Ceram. Soc. 56, 352 (1973)
- ²⁷E. L. Colla, I. M. Reaney, and N. Setter, "Effect of structural changes in complex perovskites on the temperature coefficient of the relative permittivity," J. Appl. Phys. 74, 3414 (1993).
- ²⁸A. G. Cockbain and P. J. Harrop, "The temperature coefficient of capacitance," J. Phys. D 1, 1109 (1968).
- 29E. E. Havinga, "The temperature dependence of dielectric constants," J. Phys. Chem. Solids 18, 253 (1961).
- ³⁰M. Gevers, "The relation between the power factor and the temperature coefficient of the dielectric constant of solid dielectrics," Phillips Res. Rep. 1, 279 (1946).
- 31A. Hersping, "Zur temperaturabhangigkeit der dielektrizitatskonstanten in festen stoffen," Z. Angew. Phys. (unpublished) (1966).